The Response to a Sudden Change in Indonesian Throughflow in a Global Ocean GCM

ANTHONY C. HIRST

CSIRO Division of Atmospheric Research, Aspendale, Victoria, Australia

J. S. GODFREY

CSIRO Division of Oceanography, Hobart, Tasmania, Australia

(Manuscript received 5 November 1992, in final form 21 December 1993)

ABSTRACT

The timescale and mechanisms of remote response in a global ocean GCM is investigated in the case of a sudden change in the rate of Indonesian Throughflow. In one experiment, the model is run to equilibrium with the Indonesian passage completely closed off. The passage is then opened, and the evolution of the system toward a new equilibrium is examined. In a second experiment, the model equilibrium solution with passage open is slightly perturbed by application of a body force to the water in the passage. The force is such that the change in throughflow (an increase of about 5%) has vertical profile almost identical to that of the original throughflow. The changes that evolve in the second experiment are, after appropriate scaling, quantitatively similar to those in the first, thereby verifying the approximate linearity of the response. The dynamics of this response are investigated with the aid of several idealized small-perturbation experiments, in which the model is reconfigured with a flat bottom and to be initially at rest with horizontally homogeneous density fields. It is shown that the extensive subsurface temperature responses in both the Indian and Pacific Oceans primarily result from a process of adjustment akin to baroclinic wave propagation of the first and second internal modes. The model's (approximate) first internal mode response is fairly similar to that expected from viscous linear theory. However, temperature perturbations associated with the second internal mode response are strongly distorted, in part by advection associated with the background currents. Temperature advection by the perturbation barotropic mode is unimportant except locally in the Tasman Sea and Agulhas Retroflection regions. Large differences in the patterns of response obtained previously for shallow and deep Indonesian sills, and for full versus buoyancy-driven-only throughflow, are interpreted in terms of preferential excitement of internal modes. Thus the model's baroclinic wave properties, and the spectrum of baroclinic modes excited by the throughflow change, appear very important to the pattern and timing of the subsurface (and hence surface) temperature response.

1. Introduction

Recent model studies have found that changes in the volume transport of the Indonesian Throughflow, or of the pressure distribution in its neighborhood, may result in large subsurface temperature changes throughout the model Indian Ocean basin (Godfrey and Weaver 1991; Hughes et al. 1992; Hirst and Godfrey 1993, hereafter HG). Extensive subsurface changes were also found across the Pacific basin in HG's global-model experiments. In contrast, large changes in the sea surface temperature, and hence surface heat flux, tend to be restricted to certain relatively small regions. Some of these regions are quite remote from the Indonesian passages: for example, HG found large responses in the vicinity of the Agulhas Retroflection and Outflow, the Tasman Sea, the far southeast Pacific and the far north Pacific, as well as more proximately in the equatorial Pacific and off western Australia. Hirst and Godfrey showed that each of these regions featured a mechanism whereby a large subsurface temperature perturbation was transported to the surface, namely, by wind-forced upwelling (equatorial Pacific) or by upward mixing in convective mixed layers. However, the mechanisms by which the subsurface temperature changes developed were not examined in detail.

Hirst and Godfrey dealt with changes in *steady state* circulation due to changed Indonesian Throughflow, and there was considerable discussion of the close relation between changes in the streamfunction of depth-integrated flow and the subsurface structure. Much of this discussion was motivated by expectations based on simple, linear ocean models (e.g., Anderson and Gill 1975; McCreary 1980). In these models, the steady-state response to a steady wind forcing is achieved by the passage of a series of waves through the system. First the barotropic waves pass through quickly, then a succession of internal (baroclinic) waves

Corresponding author address: Dr. Anthony C. Hirst, CSIRO Division of Atmospheric Research, Private Bag No. 1, Mordialloc, Victoria, 3196 Australia.

E-mail: ach@dar.csiro.au

of steadily higher vertical mode number follow at progressively slower speeds. The vertically integrated transport as given by the Sverdrup relation is achieved as soon as barotropic adjustment is complete. Thereafter, the passage of each successive internal wave front shoals the flow. In a linear model with no vertical mixing, the final steady-state features a confinement of the Sverdrup flow entirely to the top layer, with the velocity contributions of all the modes exactly canceling at all deeper levels (e.g., McCreary 1980). Such extreme shoaling is not observed to occur in either the real ocean or in ocean GCMs. In more complete models, the internal modes are affected by nonlinear and diffusive effects (e.g., Rhines and Young 1982; Luyten et al. 1983; Luyten and Stommel 1986; McCreary et al. 1994), and these effects increase with the vertical mode number. In practice, only the first one or two internal modes may approach their ideal final solutions everywhere. The summation of these final low-order modes, together with weak diffusion of momentum in the vertical (Rhines and Young 1982), then produces a relatively deep approximate "depth of no motion" below which velocities are very small. This provides a plausible explanation for the observed fact that a rather deep (1–2 km) "depth of no motion" is a useful approximation outside polar regions, so that the mass transport of the *steady state* flow is mainly carried by thermal winds above this depth. However, this explanation is at best a useful first approximation in the real ocean, with its complex topography and horizontal inhomogeneity, in addition to its nonlinear, convective, and diffusive behavior.

The present paper presents a more detailed study of the mechanisms underlying the subsurface temperature response to changes in the Indonesian Throughflow. The linear model response to a sudden enforced change in the Indonesian Throughflow is analogous to that discussed above for the sudden imposition of wind forcing. A barotropic wave would quickly radiate away from the throughflow region, followed by a succession of baroclinic waves. By following the transient processes by which the GCM achieves its equilibrium state, we are able to test how useful the simple linear picture is, and we achieve a clearer idea of the mechanisms and timescales involved in the establishment of the final steady state. To aid in this process, we compare the GCM's evolution to that in several experiments designed to illustrate the model's ideal internal mode response to change in the throughflow. The most practical application of our work is in the study of the response of the Indian and Pacific Oceans to *transient* fluctuations of the Indonesian Throughflow. More generally, the present work, together with that of HG, examines some basic mechanisms by which a change in surface forcing or topography may induce a *remote* response at the ocean surface. These mechanisms of remote response are likely to be more widely applicable to other experiments involving changes in model forcing/topography.

The paper is organized as follows. Section 2 gives details of the model experimental procedure. Section 3 presents the results of the full model experiments. Section 4 interprets these results with reference to the idealized internal mode experiments. Section 5 provides further discussion on dynamical processes involved in the response. Some discussion of the wider implications of the present results is presented in section 6.

TABLE 1. Vertical spacing used in the experiments (depths in meters); also background temperature and salinity profiles used in the simplified model experiments.

Model layer	Depth of middle	Temperature (°C)	Salinity (psu)
1	13	24.49	34.94
2	38	23.07	34.97
3	70	23.38	35.04
4	125	22.10	35.14
5	215	19.98	35.26
6	370	17.06	35.29
7	635	13.66	35.10
8	1025	9.99	34.75
9	1575	7.00	34.50
10	2350	5.22	34.43
11	3250	3.21	34.33
12	4150	3.03	34.32

TABLE 2. Standard values of model diffusivities and viscosities.

Parameter	Symbol	Value
Horizontal diffusivity	A_{TH}	1×10^3 m^2 s^{-1}
Horizontal viscosity	A_{MH}	1×10^5 m^2 s^{-1}
Vertical diffusivity	A_{TV}	1×10^{-4} m^2 s^{-1}
Vertical viscosity	A_{MV}	20×10^{-4} m^2 s^{-1}

2. Experimental procedure

a. Full model experiment

The global ocean model used here is the same as that used by HG. The model is based on the Bryan–Cox code (Cox 1984). The horizontal grid spacing is 1.5928° latitude by 2.8125° longitude. The model has 12 levels unequally spaced in the vertical, at depths listed in Table 1. Viscosities and diffusivities are in general spatially constant, with the values listed in Table 2. The vertical diffusivity is enhanced to 10 m^2 s^{-1} in regions of static instability in order to simulate rapid convective mixing. All climatologies used in the model surface forcing are constant annual mean. Wind stress is that of Hellerman and Rosenstein (1983). Heat fluxes are computed from bulk formulas using the model's SST (i.e., top-level temperature) and surface air temperature and specific humidity from Esbensen and Kushnir (1981). The net radiation flux of Esben-

sen and Kushnir (1981) is also used. The surface salinity is relaxed back toward Levitus (1982) values, with a time constant of 40 days. Discussion of the model, the forcing, and the model climatology are provided in HG.

Two experiments are conducted with the full GCM. The first experiment examines the evolution of the solution from HG's passage-closed case to their equilibrium passage-open case, subsequent to a sudden opening of the Indonesian passage. The second experiment examines the response following a small induced increase in the throughflow. The two experiments together indicate the extent to which the response is linear, which has implications for its dynamical interpretation, and also for the extent to which the pattern of response may be scaled up or down to correspond to throughflow changes of realistic magnitude.

In the first experiment, we begin with the equilibrium solution for the closed passage obtained by HG (their Run 2). The model was then restarted with the Indonesian passage open as per Run 1 of HG (the sill depth is 800 m). The method of restart was to initialize the revised model with the temperature (T) and salinity (S) values from the equilibrium passage closed solution, with values at new ocean points inserted via horizontal linear interpolation. The T and S fields were then held constant while velocity fields were allowed to spin up for 18 days, using a time step of 1.5 hours for both the baroclinic velocity component and the barotropic streamfunction. Net circulation was permitted around Australia. By the end of this 18-day spinup, the velocity fields were very similar to those of the equilibrium passage-closed solution, with the sole exception being a change in the barotropic streamfunction, primarily in the Australia/South Indian Ocean region [including a net circulation about Australia/New Guinea of 26 Sv (Sv $\equiv 10^6$ m^3 s^{-1})]. This "instantaneous" change in the streamfunction is the rigid-lid model equivalent of the very rapid barotropic mode response that would be expected for the real ocean. Since the perturbation barotropic flow is spread evenly over the full depth of the ocean, the effect upon *total* velocity fields is mostly small (typically about 0.005 m s^{-1}). Following this 18-day spinup, the model was integrated for 20 years using a 1.5-hour time step for all variables, including T and S. Thereafter, the model was sped to equilibrium using large T–S time steps as discussed in HG (after Bryan 1984). This experiment will be referred to as the "passage-open" run.

In the second experiment, the model is restarted from the equilibrium passage-open solution. A body force is applied to the water in the Indonesian passage, so as to increase the throughflow by about 5% (or 0.9 Sv). The vertical profile of this force is chosen so that the relative vertical profile of the throughflow change is very close to that of the original throughflow. The model was integrated for seven years using 1.5-hour time steps, and thereafter sped to equilibrium. This experiment will be referred to as the "enhanced-throughflow" run.

b. *Simplified model experiments*

In interpreting aspects of the model's transient response in terms of internal mode dynamics, we cannot rely on results from ideal shallow-water equation theory. For example, Wajsowicz (1986) and Wajsowicz and Gill (1986) have shown that transient internal mode signals are damped and have their phase speed altered by the coarse-resolution Arakawa B grid of the model. In addition, the signals are affected by the diffusivities and viscosities. We therefore construct a simplified version of the global model that allows documentation of the internal mode characteristics relevant to the present grid and mixing coefficients.

In formulating the simplified model, we retain the three-dimensional grid and the geometry of the World Ocean, but the depth of the ocean floor is set to 4600 m everywhere. Continental boundaries in the Tropics and Southern Hemisphere were modified to represent the 800-m isopleth in the full model. A simplified Indonesian passage is retained (e.g., see Fig. 11a). Initially, the ocean is at rest with T and S horizontally uniform and having the vertical profiles shown in Table 1. These profiles correspond to zonally averaged Indian Ocean values at 22°S in the passage-closed case. To prevent vertical diffusion from quickly modifying the initial profiles, a relaxation is performed toward particular profiles chosen to ensure that the initial T and S profiles are exactly maintained outside regions affected by internal mode motions. (The required relaxation profiles are quite different to those of Table 1 and were computed via solution of the diffusion equation.) The relaxation timescale is set at 30 days for the top level and 400 years for all lower levels. The short top-level relaxation time is chosen so as to mimic the short effective Haney-relaxation time constant of the top level in the full model. The lower-level relaxation time is found by experiment to be sufficiently slow that it little affects the internal mode response. Bottom friction is set to zero, but the no-slip condition for the lateral boundaries is retained. The horizontal and vertical diffusivities and viscosities are spatially constant, with the same values as for the full model in statically stable conditions (Table 2). A consequence of the vertically constant A_{TV} and A_{MV} is that the vertical modal structure will not be exactly preserved as the wave front propagates away from the source region, that is, the modes are no longer strictly separable (McCreary 1980; Wajsowicz 1986). However, we find that the structure of first and second internal mode motions are fairly closely preserved in our simplified model.

The model's internal mode characteristics may now be investigated by prescribing a localized heat source or body force of vertical profile relevant to the mode under study, and examining the behavior of the re-

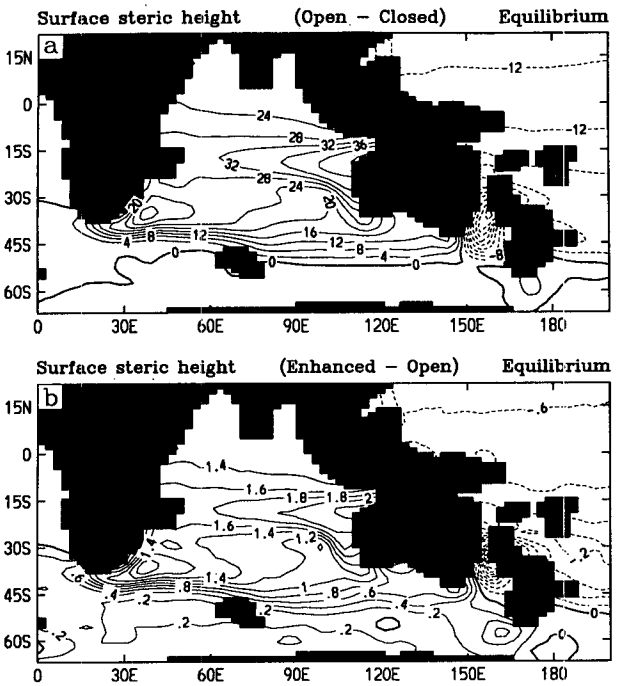

FIG. 1. Surface steric height difference after equilibration for (a) passage-open solution minus passage-closed solution and (b) enhanced-throughflow solution minus passage-open solution. Units are in centimeters; negative contours are dashed. A depth of zero perturbation motion at 2800 m is assumed.

sulting wave signal. In the present paper, we show in detail the results of two such experiments, designed to investigate the separate responses of the first and second internal modes to a pattern of forcing that partly resembles that incurred by the full model in the opening of the Indonesian passage. In both experiments, a body forcing term is added to the momentum equations. The force is applied only in the meridional direction, and only across the Indonesian passage directly to the east of the model's "Java Peninsula." The magnitude of the force is very small, to ensure that nonlinear effects are negligible. No other force is applied to the model. For the first experiment, the body force has a vertical profile corresponding to that of the velocity profile for the first internal mode. The model is run from rest for 8 years with 1.5-hour time steps. Thereafter, the solution is sped to equilibrium as per the full model. The run was ended after 110 years integration (for T–S fields), by which stage changes in the model fields had practically ceased. The second experiment is similar, except that the body force has vertical profile corresponding to that for the second internal mode. In section 4, the transient and final steady patterns of the simplified model solutions are compared to those of the full model, where the internal mode response may be modified by bottom topography, advection by background-state currents, inhomogeneous density profiles, and deep convective mixed layers.

3. Results of full model runs

Figure 1 compares the equilibrium changes in surface steric height in the full model induced by (a) opening the Indonesian passage and (b) forcing the slight increase in the throughflow. The pattern in Fig. 1a is consistent with the surface current changes described in detail in HG. The changes in Fig. 1b are clearly similar to those in Fig. 1a, after appropriate scaling. Such similarity is also found throughout the course of the respective transient evolutions. This similarity verifies that the responses discussed in HG and here are approximately linear. The remainder of this section presents the time evolution of the response in the passage-open run. Results for the enhanced-throughflow run may be obtained approximately by dividing the changes shown by a factor of 20.

The adjustment process in the passage-open run is illustrated in Figs. 2–4, which show the departure in

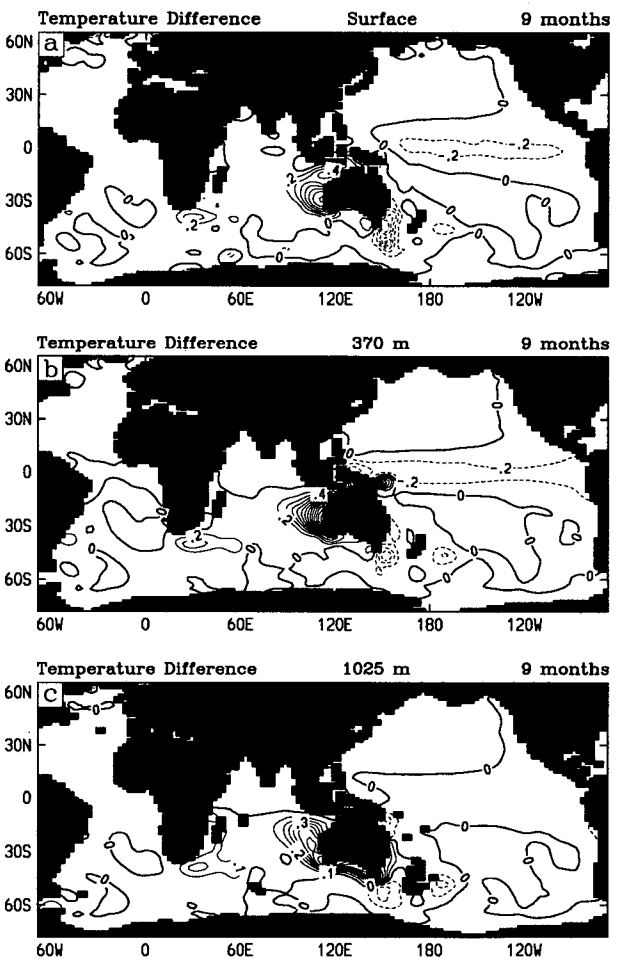

FIG. 2. Temperature difference at depths of (a) 12.5 m, (b) 370 m and (c) 1025 m for passage-open solution at 9 months minus passage-closed solution. Contour interval is 0.2°C for (a) and (b) and 0.1°C for (c). Note that the "0" contour in fact represents the −0.01°C contour, in order to reduce zero-contour clutter. Otherwise, negative contours are dashed.

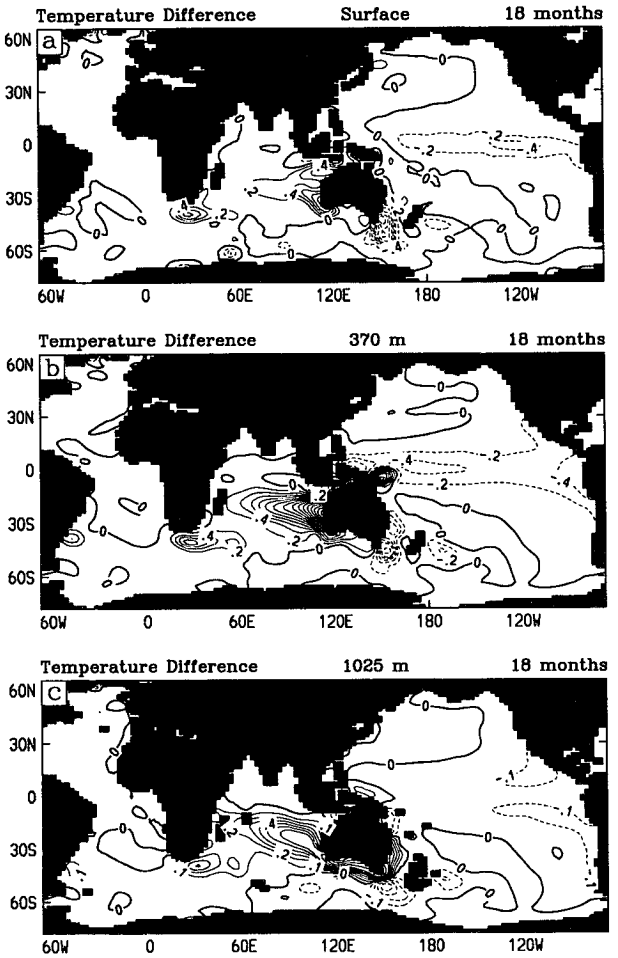

FIG. 3. Temperature difference after 18 months; otherwise as for Fig. 1.

temperature from that of the passage closed case at 9, 18, and 48 months after the opening, respectively. Departures are shown at depths of 12.5 (top level), 375, and 1025 m. The top-level departures may be compared to that for the final equilibrated solution shown in Fig. 5a. Temperature departures at the other depths after equilibration were shown in HG (their Fig. 13). Figures 5b and 5c instead show the density departures after equilibration. These density departures are very similar in pattern to those of temperature, and are more directly relevant to the dynamical discussion in sections 4 and 5. Henceforth, departures from the passage-closed solution will be referred to as "perturbations."

Clearly apparent in Figs. 2–4 is a systematic alteration of the subsurface T field, which, for the most part, spreads steadily outward from the Indonesian passage. Note in particular the rapid spread of the positive perturbation signal down the west coast of Australia, and its subsequent slow extension westward across the Indian Ocean. Note also the rapid spread of the negative perturbation signal eastward along the equatorial Pacific waveguide and then poleward along the American west coast, and its eventual slow spread westward back across that ocean basin.

In contrast to the steady progression of the subsurface temperature perturbations, the barotropic streamfunction undergoes substantial large-scale changes immediately following the opening of the passage, as shown in Fig. 6. The early extensive response of depth-integrated flow (Figs. 6a,b) has little or no signature in the subsurface temperature fields (e.g., Figs. 2, 3), and thus the associated velocity perturbations are nearly constant right down to the bottom topography. The response only partly resembles that expected for a flat-bottom ocean model (e.g., HG or Fig. 12a here), and shows evidence of severe distortion by the bottom topography. For example, the imprint of the Ninety-East Ridge (at 90°E) and the Mascarene Ridge (at 60°E) is apparent on the westward flow from the passage in Fig. 6a. The arrival of the temperature signal provides horizontal density gradients that may shoal the depth-

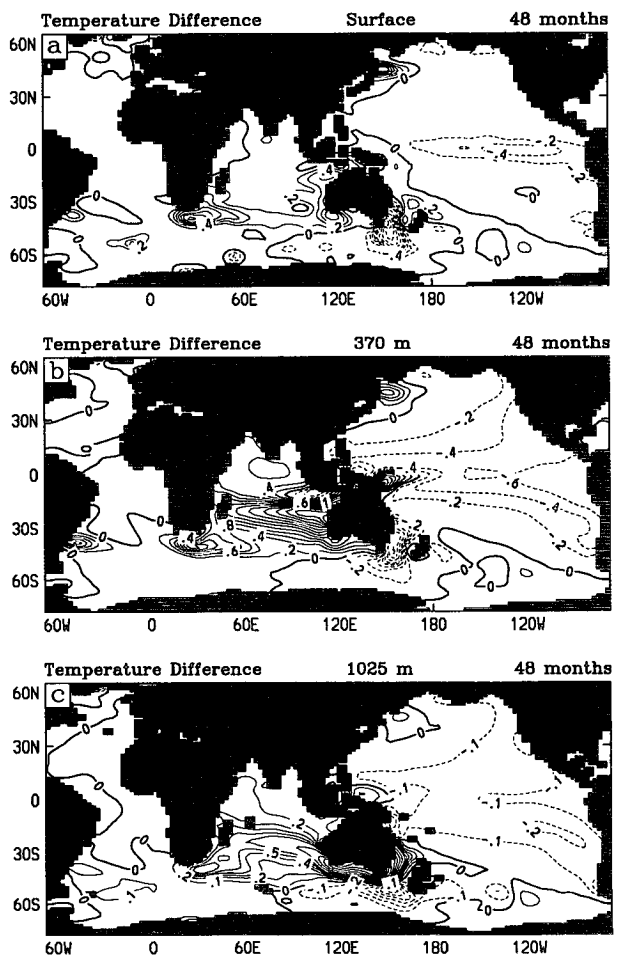

FIG. 4. Temperature difference after 48 months; otherwise as for Fig. 1.

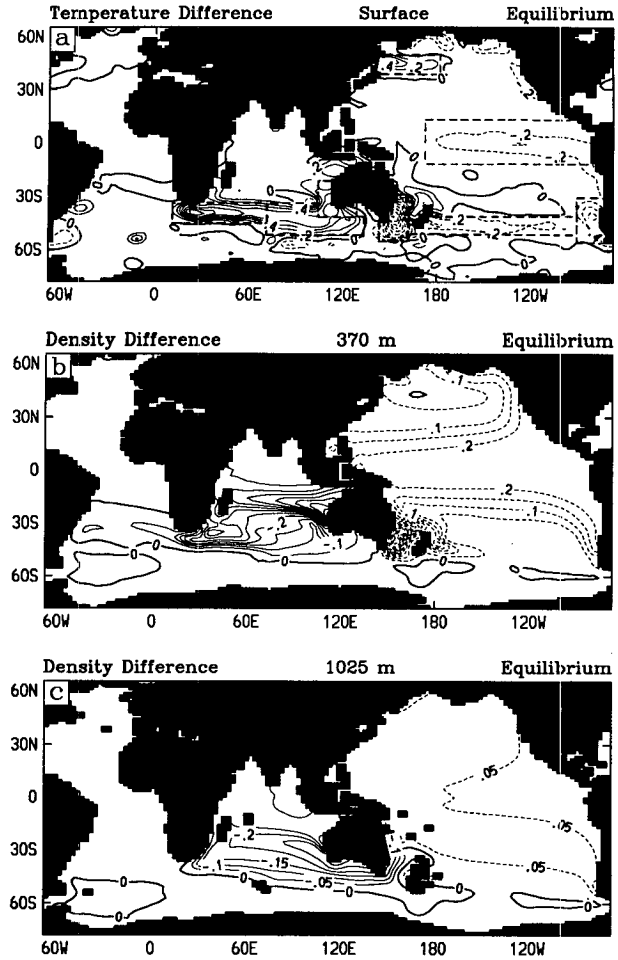

FIG. 5. Top panel (a) shows equilibrium temperature difference at 12.5-m depth, and boundaries of areas used for spatial averaging of SST (long dash). Lower panels (b, c) show density differences between the equilibrium passage-open and passage-closed solutions at 370 m and 1025 m, respectively; contour interval is 0.05 kg m^{-3} and positive contours are dashed.

integrated flow, and reduce the impact of bottom topography (Fig. 6c, HG's Fig. 11a).

One potential means by which the subsurface temperature signal may spread away from the Indonesian passage is via direct horizontal advection. After the opening, warm west Pacific water may be advected into the Indian Ocean by the *total* flow, and then westward by the South Equatorial Current. A second means of subsurface temperature change is via internal mode propagation. Certainly the pattern of the Indian Ocean signal is reminiscent of such propagation (e.g., Godfrey and Golding 1981). Characteristic timescales of the two mechanisms may be compared. After the initial barotropic adjustment, westward current speeds in the upper 270 m between 13° and 17°S (near the core of the South Equatorial Current) grade from a mere 0.012 m s^{-1} in the eastern to about 0.08 m s^{-1} in the western Indian Ocean. A summation of grid box transit time yields an advective timescale of order 90 months for the signal to extend from the Indonesian passage westward to the Madagascar coast. Currents at greater depth are weaker and yield still longer timescales. In contrast, the first internal Rossby mode at similar latitude propagates at about 0.14 m s^{-1} and takes only about 18 months to reach Madagascar (section 4), which corresponds closely in timing to the signal in Figs. 2 and 3.

Next, we note that internal mode adjustment in a linear model contributes to subsurface warming solely by vertical advection, and not by horizontal advection. Therefore, the relative magnitudes of the perturbation vertical advection $[(wT_z)']$ and horizontal advection $[(uT_x + vT_y)']$ provide a useful indicator of the mechanism of subsurface temperature change. Figure 7 shows the separate contributions of perturbation vertical and horizontal advection to the temperature tendency at 370-m depth, 9 months after the opening (the contributions of nonadvective terms are mostly small).

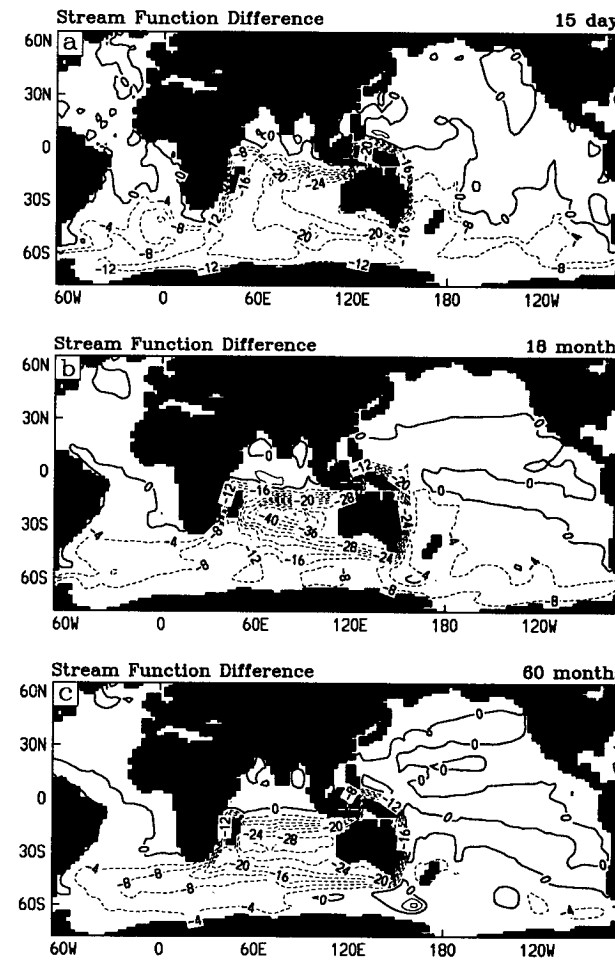

FIG. 6. Streamfunction of depth-integrated perturbation flow at (a) 0.5, (b) 18, and (c) 60 months after opening the passage. Contours are at intervals of 4 Sv.

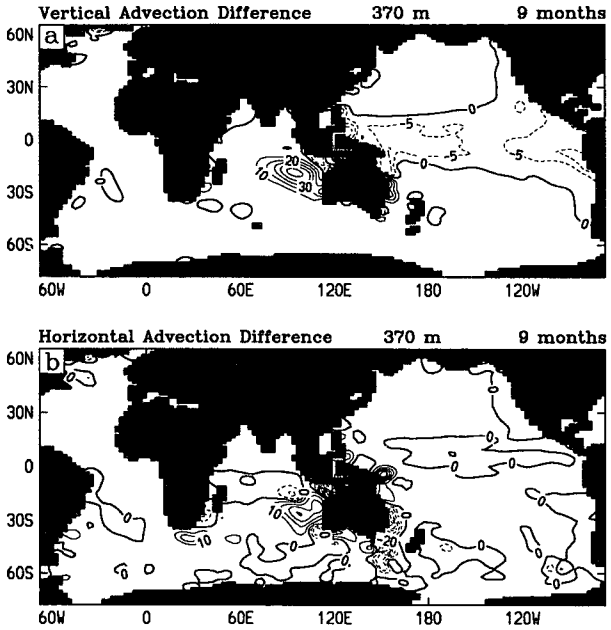

FIG. 7. Difference in (a) vertical temperature advection $(w\partial T/\partial z)'$ and (b) horizontal temperature advection $(u\partial T/\partial x + v\partial T/\partial y)'$ for passage-open case after 9 months minus passage-closed case, at 370-m depth. Contour interval is 10×10^{-9} °C s^{-1} except that the -5×10^{-9} °C s^{-1} is also shown. Note that the "0" contour in fact represents the -0.5×10^{-9} °C s^{-1} contour in order to reduce zero-contour clutter. Otherwise, negative contours are dashed.

Vertical advection dominates the main temperature change fronts in the Pacific and, to a lesser extent, in the Indian Oceans (Fig. 2b). This dominance is more pronounced at 1025 m (not shown), especially in the Indian Ocean. These results are consistent with internal mode propagation being the primary cause of the spread of temperature change across both ocean basins.[1]

Horizontal advection does dominate in several smaller regions, including the Agulhas Retroflection, southwestern Tasman Sea, and immediately to the northeast of New Guinea (Fig. 7). In all of these regions the barotropic flow perturbation (Fig. 6) cuts across closely spaced isotherms, and so contributes to the subsurface temperature change. [To the northeast of New Guinea, a subsurface front separates water of the South Equatorial Current from fresher and cooler water of Mindanau origin (e.g., Godfrey et al. 1993).]

The early SST response shown in Figs. 2a and 3a reveals rapid development of SST perturbations near the west Australian coast, in the Tasman Sea, and along the equatorial Pacific. These are three of the regions identified by HG as having a large equilibrium response at the surface (see Fig. 5a here). The three regions are characterized by the rapid development of subsurface temperature perturbations following the opening, as discussed above, and the communication of the subsurface perturbation to the surface by convective mixing (west Australian coast and Tasman Sea) or wind-forced upwelling (equatorial Pacific). The SST change off the west Australian coast at 9 months is enhanced as a result of initially strong southward flow associated with the near-coastal subsurface warming. Later perturbation motion there is weaker, so meridional temperature advection is less and the perturbation SST declines somewhat.

SST perturbations take longer to develop in other areas noted in HG. Eight areas of large equilibrium response are delineated by the boxes shown in Fig. 5a. The SST change averaged over each of these boxes is shown in Fig. 8 as a function of time. The time elapsed before full development of the SST change varies greatly, from less than 12 months in the case of the Leeuwin Current region and equatorial Pacific, to about 20 years in the case of the eastern Agulhas Outflow and southern Pacific regions.

The immediate initiation of SST change in the Tasman Sea points to the important role played by horizontal advection associated with the barotropic response in that region. A barotropic current along the southeast coast of Australia of depth 3700 m (levels 1–11), width 400 km, and strength 16 Sv (e.g., Fig. 6a), yields a velocity of 0.01 m s^{-1}, which, acting on a typical longshore temperature gradient of 5×10^{-6} °C m^{-1} (e.g., HG's Fig. 9e), yields a cooling rate of 2°C y^{-1}, consistent with the largest rates of Tasman Sea cooling evident in Figs. 2a and 3a. This cooling is strongest in the upper 500 m, where longshore temperature gradients are largest.

The use of fixed surface air temperature and specific humidity in the present simulations assumes no adjustment of the atmospheric boundary layer to underlying SST changes. In reality, partial adjustment would occur, which may allow for larger or more extensive SST perturbations.

A prominent feature of the Indian Ocean response at equilibrium is a jetlike perturbation current, which arcs east then southeast from near Madagascar to the southwest coast of Australia where it is associated with enhanced surface heat loss and coastal downwelling (HG, also Fig. 1 here). This surface flow feature is underlain (at depths 400–1500 m) by a return flow toward the northwest/west. This flow/underflow pair coincides with the southern boundary of a band of large upper-ocean density or temperature perturbation (Fig. 5b, HG's Fig. 13a) centered at about 20°S. The establishment of the flow/underflow pair is illustrated in Figs. 9a–c. An underflow is first evident at about 9

[1] The perturbation vertical advection $(wT_z)'$ may be split into two subterms, $w'\bar{T}_z$ and $(\bar{w} + w')T'_z$, where the overbar indicates fields in the passage-closed case, and prime indicates perturbations away from those fields. Internal mode adjustment in a linear model, in fact, contributes via only the first subterm. However, we find that the second subterm is relatively small, and the conclusion regarding the dominant effect of internal mode propagation stands.

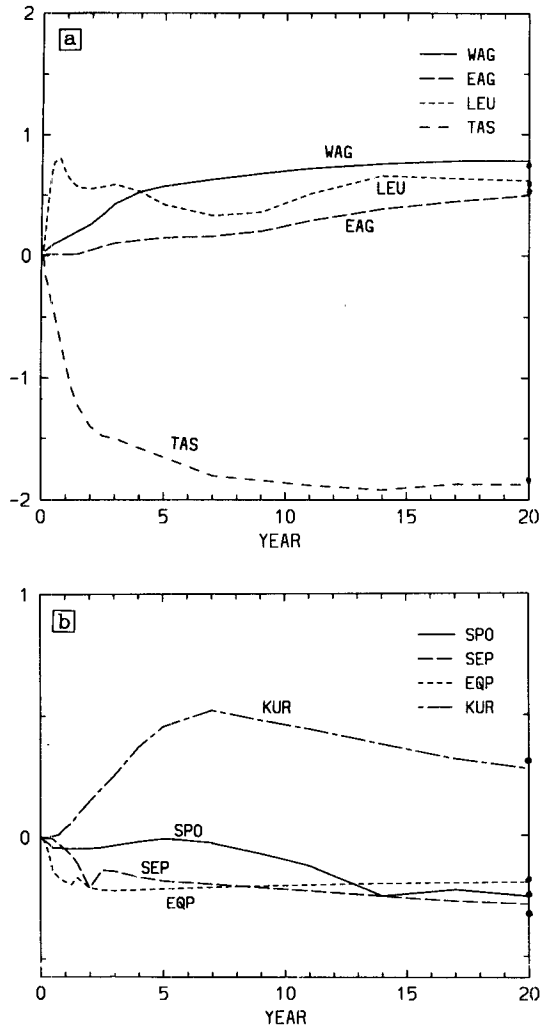

FIG. 8. Changes in SST during first 20 years of the passage-open case averaged over each of eight regions delineated in Fig. 5a. WAG: Agulhas Retroflection/West Agulhas Outflow (15°–70°E), EAG: East Agulhas Outflow (70°–130°E), LEU: Leeuwin Current region, TAS: Tasman Sea, EQP: equatorial Pacific, SPO: band across far south Pacific, SEP: region in far southeast Pacific, KUR: region in far northwest Pacific. Equilibrium differences (open minus closed) indicated by dots on right of figure.

months, near the west Australian coast (Fig. 9a). It then extends westward, reaching Madagascar at about 24 months (Fig. 9b). Thus the underflow extends westward at about the same rate as the primary temperature/velocity signal, but lags roughly six months behind. The underlying dynamics are not immediately obvious; the flow reversal is too shallow for the first internal mode, while westward propagation appears too rapid for the second internal mode (see section 4). Flow/underflow pairs also occur along the zones of sharp density gradient evident in Fig. 5b in both North and South Pacific (HG). Their dynamics are further discussed in sections 4 and 5.

4. Results of experiments with simplified model

This section presents a comparison of the full model results with those of the simplified model, to further test the extent to which the full model response may be interpreted in terms of the linear internal modes. In such an interpretation, an increase in southward flow over the shallow Indonesian sill would result in convergence of upper-level water in the throughflow exit region northwest of Australia, and consequent subsurface warming (pycnocline deepening) of that region. Conversely, subsurface cooling would be expected in the throughflow entrance region of the far west Pacific. These pycnocline perturbations would then extend away from the Indonesian passage as internal mode wave fronts.

The general stratified linear model, and its decomposition into vertical modes, has been thoroughly treated by many authors (e.g., McCreary 1980; Gill 1982). Motions in such a model may be decomposed into a set of orthogonal vertical modes, each of form

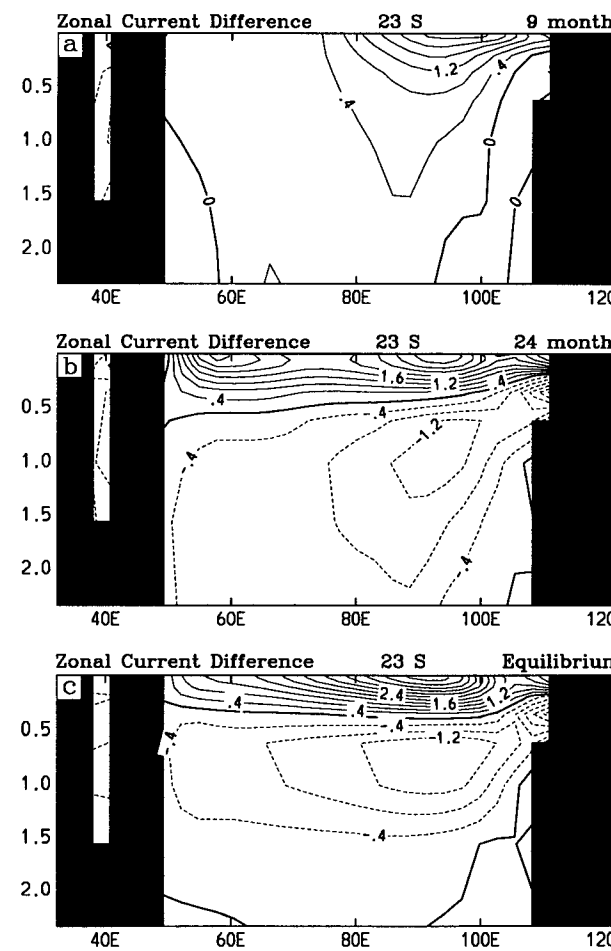

FIG. 9. Sections showing perturbation zonal motion at 23°S at (a) 9 months and (b) 24 months after opening of the Indonesian passage and (c) equilibrium difference. Contour interval is 0.004 m s^{-1}.

$$(u_n, v_n, p_n, \rho_n) = (U_n(x, y, t)Z_n(z), V_n(x, y, t)Z_n(z), P_n(x, y, t)Z_n(z), \rho_n(x, y, t)Z'_n(z)). \quad (1)$$

Here u_n, v_n, p_n, and ρ_n are the zonal and meridional velocity, pressure, and density perturbations, respectively, of the nth mode. The set of vertical modes includes a barotropic mode ($n = 0$), which features vertically constant horizontal motion, and a series of internal modes ($n = 1, 2, 3, \cdots$), whose functions of vertical structure Z_n obey

$$\frac{d}{dz}\left(\frac{1}{N^2}\frac{dZ_n}{dz}\right) + \frac{1}{c_n^2}Z_n = 0, \quad (2)$$

where $N(z)$ is the Brunt–Väisälä frequency and c_n is an eigenvalue that corresponds to the gravity wave speed for that mode. Upon excitation by a body force of profile $Z_n(z)$, the evolution of the horizontal fields (U_n, V_n, P_n) for each vertical mode is governed by the standard shallow-water equations. We finally note that ρ_n has the same horizontal pattern as P_n, since density and pressure are related via the hydrostatic equation.

Approximate internal mode characteristics of the model were first investigated by solving (2) via a shooting method, for several typical model density profiles including that from Table 1. Boundary conditions applicable to the rigid lid and a flat ocean bottom were used (Moore and Philander 1977). For the density profile from Table 1, we obtain $c_1 = 3.2$ m s^{-1} and $c_2 = 1.8$ m s^{-1}, which are reasonably close to values calculated for typical observed tropical profiles. Apparently the effect of the model's excessively deep thermocline (which increases the c_n) is being partly offset by the unrealistically low density of the deep water.

The present simplified model differs from the ideal stratified model because of the spatially constant vertical diffusivity and viscosity and the top-layer Haney condition. Mode-like structures more exactly relevant to the simplified model were therefore deduced by direct experiment. Body forces were applied in the zonal direction to the model's far west equatorial Pacific. A distinct separation of mode-like structures occurred, with first mode–like perturbations extending rapidly eastward along the equatorial waveguide, and second mode–like perturbations extending eastward much more slowly. The vertical profiles of these structures were found to be well preserved during their eastward passage. Profiles of velocity, density, and temperature perturbations for the first and second mode–like structures were determined by inspection of solution and are shown in Fig. 10. These profiles differed only slightly from those determined earlier by the shooting method. The usefulness of the profiles in Figs. 10a and 10c in generating pure modal responses was tested by applying body forces of corresponding profile to the model's west equatorial Pacific. In both cases, the resulting modal signal was almost pure during the first six months of integration. Thus the model's A_{MV} and A_{TV} have little effect on the *initial* response of the low-order modes to a given forcing, but we may expect their effect to increase as the integration proceeds.

The mix of internal modes excited by a change in throughflow depends on the vertical profile of the change in flow entering or exiting the Indonesian passage (McCreary and Kundu 1986). In an ideal linear system, such a perturbation flow would project onto the vertical modes such that the sum of the modal velocity profiles matches that of the throughflow change. A deep change in throughflow would project mostly onto the barotropic and first internal modes, while a shallow change would project also onto the barotropic but more strongly onto higher-order internal modes. The evolution of the system to equilibrium would involve the propagation of these modes about the global ocean.

To study the global modal response to a change in Indonesian Throughflow, the simplified model detailed in section 2b is subject to forcings designed to excite particular vertical modes. In a preliminary experiment, we verify the results of HG for the ideal response of the barotropic mode by applying a body force of vertically constant profile to the fluid in the Indonesian passage. Flow, uniform in the vertical, requires about 40 days to equilibrate, after which time the total lateral viscous drag equals the applied force. Figure 11a shows the equilibrium streamfunction, in the case where the model is subject to a forcing of strength chosen to yield a final throughflow of 17 Sv (as per the full model). The pattern in Fig. 11a is almost identical to that found by HG using a simple Munk (1950) viscous flow model. This agreement is to be expected, of course, since the diffusivities and vertical viscosity of the simplified model do not affect the barotropic mode.

In an ideal stratified model, the equilibrated internal mode motions can be shown to be nondivergent, and we may define a streamfunction ψ_n such that $U_n = -\psi_{ny}$ and $V_n = \psi_{nx}$. It may be shown that the ψ_n will form exactly the same pattern as for the barotropic streamfunction. Figure 11a therefore also gives the ideal equilibrium pattern of response for internal mode motions.

When applied to an internal mode, a pattern of ψ_n such as in Fig. 11a implies subsurface changes in the density field. The relation between ψ_n and ρ_n may be readily obtained via the thermal wind relation ($u_z = g\rho_y/\rho_0 f$). If we then assume that $\rho_n = \rho_0\alpha T_n$, where $T_n(x, y)$ is the horizontal pattern of temperature perturbation, and α is a representative value of the thermal expansion coefficient, then we obtain

$$T_{ny} = -\frac{f}{g\alpha}\psi_{ny}. \quad (3)$$

The difference in T_n across a zonal flow that is narrow relative to meridional change in the Coriolis parameter (f) is simply

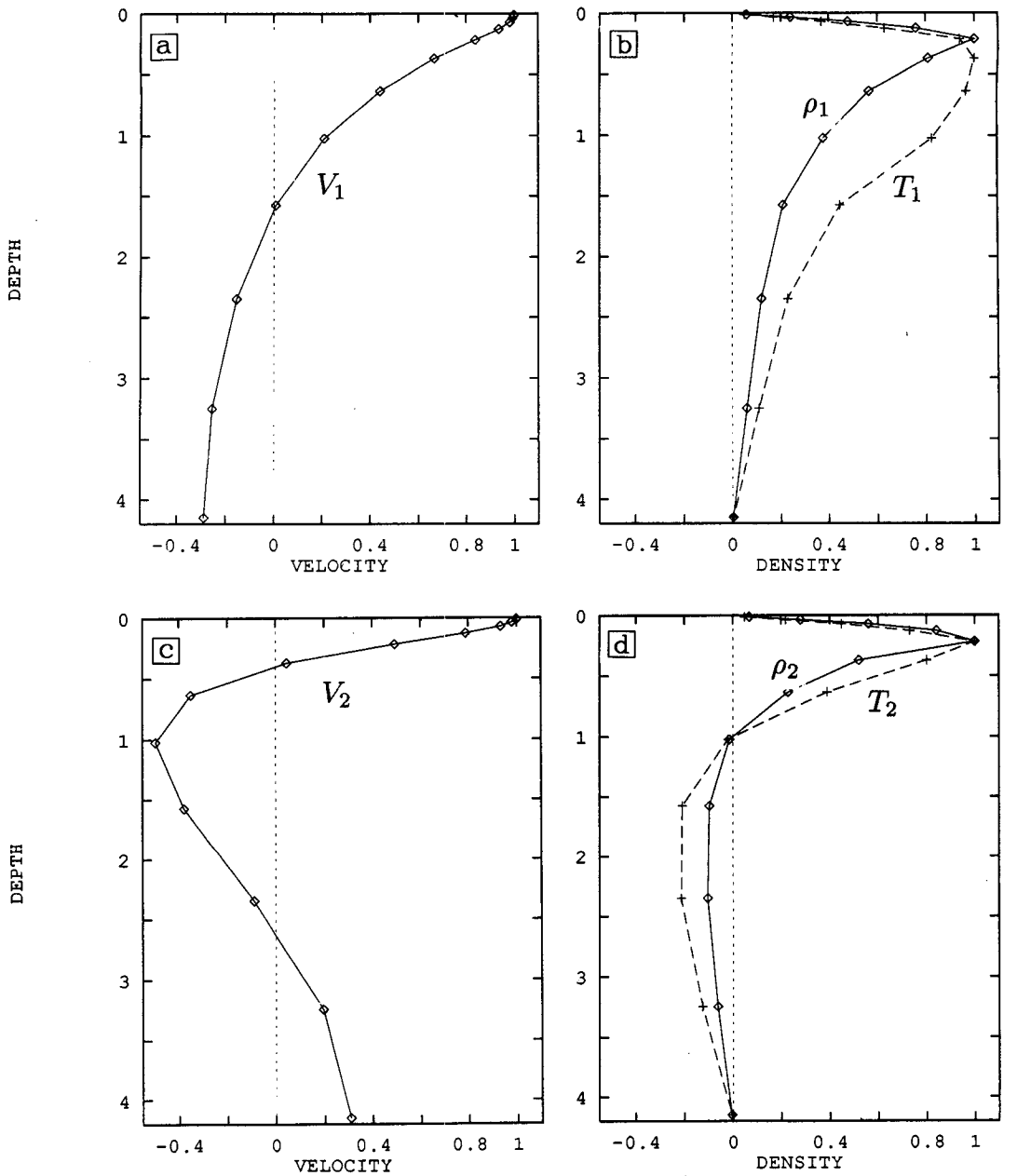

FIG. 10. Horizontal velocity (V_n), perturbation density (ρ_n), and temperature (T_n) profiles associated with first ($n = 1$) and second ($n = 2$) internal modes, as indicated by inspection of the simplified model solution in response to forcings applied to the western equatorial Pacific. The prescribed background profiles of T and S correspond to zonal averages across the Indian Ocean at 22°S (Table 1).

$$\Delta T_n = -\frac{f(y_0)}{g\alpha}\Delta\psi_n, \tag{4}$$

where ΔX denotes the difference in a variable X across the flow and y_0 denotes the latitude of the flow axis. The actual change in temperature ($\Delta T'$) across the flow is then given by $\Delta T' = \Delta T_n Z'(z)$. The important point is that the change of temperature across a given baroclinic flow is smaller at low latitudes than at high latitudes. If we approximate the pattern in Fig. 11a by the simplified pattern in Fig. 11b, we may calculate the global temperature response (T') to within a global additive constant. Interbasin temperature differences so calculated at 370-m depth are shown in Fig. 11b for the case of a first internal mode featuring an upper throughflow of 10 Sv. Relative to the Pacific and Southern Oceans, the southern Indian Ocean warms strongly, the northern Indian and the far south Atlantic

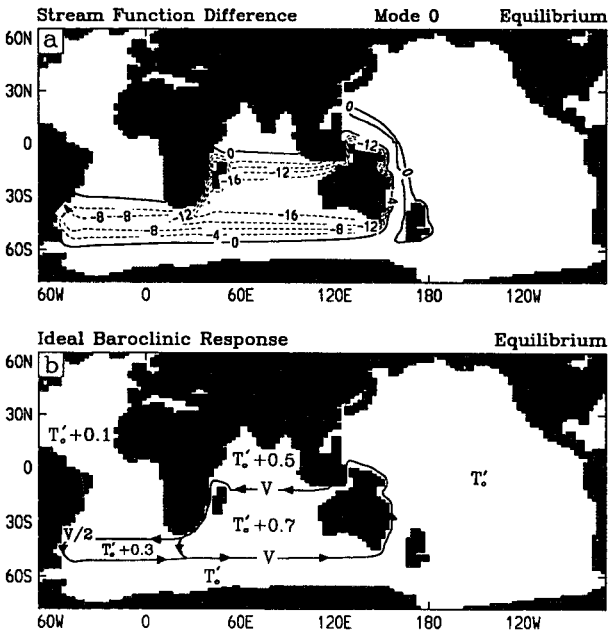

FIG. 11. (a) Streamfunction for barotropic flow in simplified model subject to barotropic forcing in the Indonesian passage. Contour interval is 4 Sv. (b) Idealized pattern of upper flow for internal mode response. Also shown are the temperature changes at 370 m associated with such a first internal mode response featuring an upper throughflow (V) of 10 Sv. Changes are in degrees Celsius and are relative to that in the Pacific and Southern Oceans (T_0').

Oceans warm moderately, and the remainder of the Atlantic warms very slightly (see also discussion in HG).

We now examine the actual response of our simplified model to a forcing in the Indonesian passage designed to excite a first internal mode response. Figure 12 shows the temperature response at 370-m depth after 18 months following switch-on of forcing. Indian Ocean warming involves the propagation of a coastal Kelvin wave signal counterclockwise about Australia, and its subsequent westward radiation as a Rossby wave signal. Pacific cooling involves a Kelvin signal along the equatorial waveguide, its subsequent poleward propagation along the American west coast, and westward radiation as a Rossby signal. The response is similar in pattern and timing to the primary signal evident in the full model (e.g., Figs. 3b,c). Some differences are noted; for example, the warming signal in the full model is only weakly apparent along the southern Australian coast, at 370-m depth, while along the eastern Australian coast, it is dominated by the cooling advective effects discussed previously.

We may compare the propagation speeds of the wave fronts in the simplified model with that expected from ideal theory. The largest inconsistency involves the propagation speed of coastal Kelvin waves. The cooling signal is found to extend down the west coast of South America at about 0.5 m s^{-1}, much slower than the 3.2 m s^{-1} expected based on the direct solution of (3). Such distortion is foreshadowed by the analysis of Wajsowicz and Gill (1986) and results partly from the zonal model grid spacing (of order 300 km) being much greater than the Rossby deformation radius (of $c_1/f \sim 40$ km). Otherwise, the negative T signal extends eastward in the equatorial Pacific at about 2.8 m s^{-1}, close to the 3.2 m s^{-1} expected for the equatorial Kelvin wave. In this case, the model's meridional resolution (175 km) is less than the equatorial deformation radius (of $c_1/(2\beta)^{1/2} = 260$ km). The positive T signal at 15°S propagates across the Indian Ocean at 0.14 m s^{-1} close to the value of $c_R = \beta c_1^2/f^2 = 0.15$ m s^{-1} expected for the long planetary waves (Gill 1982).

The final equilibrium response in the simplified model (Fig. 13a) yields a slightly cooler Pacific, and interocean temperature differences are qualitatively consistent with the ideal schematic in Fig. 11b. [One discrepancy is the minimal temperature change in the far Southern Ocean, when compared to the Pacific.] However, some diminution of the signal is evident with distance away from the western continental coasts. This diminution decreases slightly with depth; thus the vertical profiles of perturbation temperature are not exactly uniform over the domain. Apparently, the upper levels lose heat via diffusion and surface heat loss as the Rossby wave signals propagate slowly westward.

The evolution of the simplified model following a switch-on of the second mode forcing in the Indonesian passage is qualitatively similar to that of the first mode. Coastal Kelvin wave signals are even more severely slowed by the resolution, advancing at just 0.15 m s^{-1}. Other signals advance at rates close to those expected from ideal theory using a gravity wave speed of 1.8 m s^{-1}. The Indian Ocean Rossby signal first reaches Madagascar after about 50 months.

The final equilibrium temperature response to the second mode forcing is shown in Fig. 13b. Attenuation is significantly more rapid than for the first mode, as expected because of the slower propagation speed and more complex vertical structure. An estimate of the attenuation rate due to vertical viscosity (Table 2) based on the profile in Fig. 10c yields a decay length

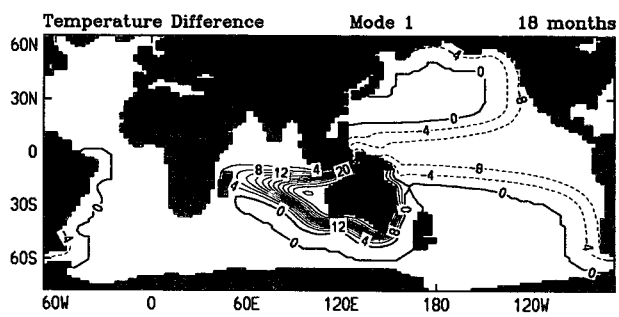

FIG. 12. Temperature perturbation in simplified model solution at 18 months after switch-on of first mode forcing at 370-m depth. Contour interval is 4×10^{-3} °C.

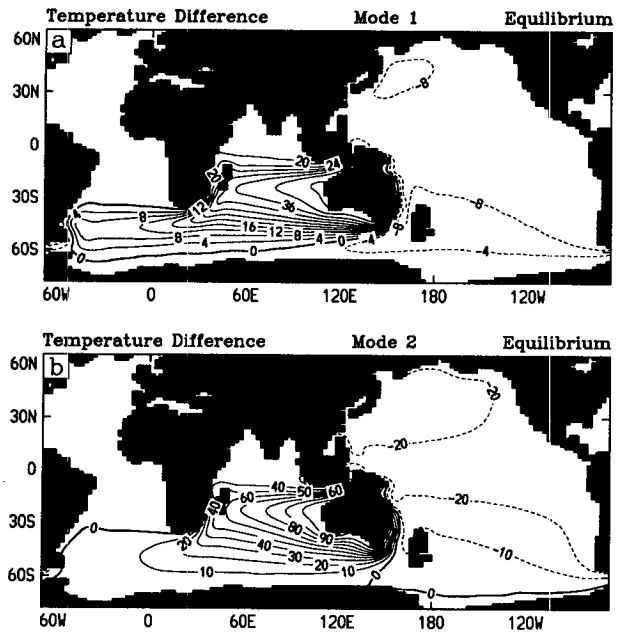

FIG. 13. Final equilibrium temperature perturbation in simplified model subject to steady forcing of (a) the first mode and (b) the second mode at 370-m depth. Contour interval is 4×10^{-3} °C in (a) and 10×10^{-3} °C in (b). Upper throughflow in (a) is 0.7 Sv (cf. Fig. 11b).

scale of only about 12 degrees of longitude at 20°S. A similar estimate for vertical diffusivity yields a decay length scale of about a factor of seven greater. The actual decay length scale is closer to the latter, presumably because the available potential energy of such large-scale signals is much greater than the associated kinetic energy.

A comparison between the equilibrium response of the full model and the internal mode responses of the simplified model may be achieved by projecting the perturbation density field of the full model response onto the profiles in Figs. 10b and 10d. The resulting first mode projection (Fig. 14a) shows signals that extend fairly uniformly across the ocean basins, in a pattern broadly similar to that in Fig. 13a. The largest discrepancy involves failure of the warm signal to extend westward to the South American coast, presumably as a result of advection associated with the Antarctic Circumpolar Current in the full model (HG). (Background barotropic flow eastward is estimated to exceed the westward propagation speed of first mode Rossby waves south from about 40°S.) In contrast, the second mode projection (Fig. 14b) shows a distorted pattern, which appears unlike Fig. 13b, especially in the Indian Ocean, though it does resemble the upper-ocean density response shown in Fig. 5b. Especially notable are the rapid transitions between regions of strong and weak second mode projection. The flow/underflow pairs discussed earlier lie along these transition zones. It is noted that these flow/underflow pairs feature flow reversal at a depth similar to that for the upper flow reversal of the second mode (e.g., cf. Figs. 9c and 10c).

In the full model, internal mode structure tends to deepen at higher latitudes, as the upper-ocean stratification weakens. Thus projections as in Fig. 14 based on set modal profiles defined for tropical stratification (e.g., Fig. 10) may not accurately indicate the pattern of modal penetration at higher latitudes. We therefore recomputed the projections using modal profiles calculated for typical stratifications in the central Indian Ocean at 26°S and also at 32°S, with broadly similar results.

5. Discussion

We may conclude on the basis of the comparisons in section 4 that a large portion of the subsurface temperature response to throughflow change may be understood in terms of internal mode adjustment. However, significant discrepancies remain, and these are discussed below.

First, What is preventing the penetration of second mode–like density perturbations into the central subtropical ocean basins, thereby giving rise to the curved flow/underflow pairs? Clearly, attenuation of the wave signal by the background viscosity/diffusivity is not sufficiently rapid to do this (Fig. 13b). It was noted in HG that the flow/underflow pairs follow paths reminiscent of the solution characteristics computed by Luyten and Stommel (1986) in the "eastern regime"

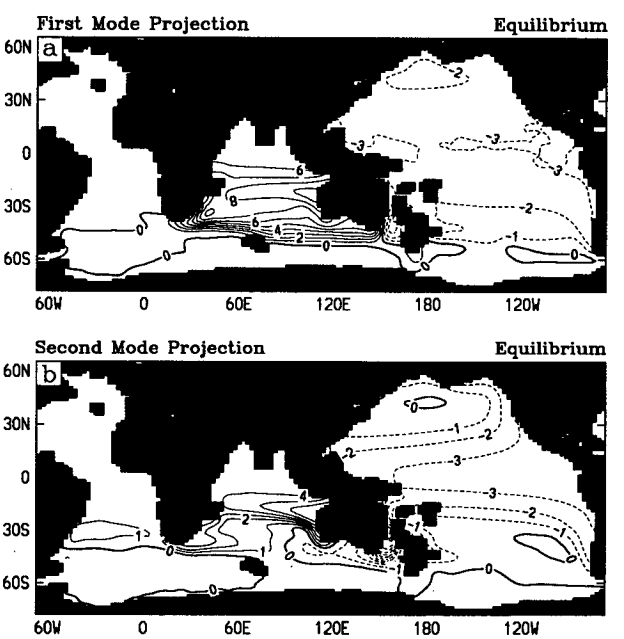

FIG. 14. Projection of the perturbation density field at equilibrium onto (a) the first mode and (b) the second mode profiles shown in Fig. 10.

of their two-layer model of the subtropical gyre. These characteristics stem from the eastern ocean boundary, and their orientation is governed by the phase velocity of nondispersive internal Rossby waves as modified by the Sverdrup transport vertically averaged over the active ocean layers. The Sverdrup flows off the subtropical/lower-midlatitude west coasts of Australia and America are directed primarily equatorward (e.g., Godfrey 1989; HG's Fig. 5), with meridional components of similar magnitude to the westward phase velocity of second mode Rossby waves. For example, northward motion at about 30°S and poleward of the flow/underflow pair in the eastern Indian Ocean tapers gradually from about 0.01 m s^{-1} in the upper 100 m to near zero below 1800 m, with an average value of about 0.0075 m s^{-1} in the upper 800 m (spanning the major second mode density perturbation). In the absence of advection, long wavelength Rossby waves propagate westward nondispersively at a speed $c_R = \beta c_2^2/f^2$. Thus at 30°S in the Indian Ocean, a typical value for c_2 is 1.6 m s^{-1}, leading to c_R = 0.01 m s^{-1}. We then might expect the characteristics for the second internal mode to follow a path angled 37° north of west. This is in reasonable agreement with the deflection evident for the flow/underflow pair (Figs. 1, 5b, 14b, and HG's Fig. 14).

The essence of the above hypothesis is that advection by the Sverdrup flow deflects the second and higher mode Rossby waves emanating from the eastern boundary so that these waves are unable to reach a large portion of the ocean interior. Support is found in a comparison of the results of Godfrey and Weaver (1991) and Hughes et al. (1992). The former apply no wind stress curl, hence have no Sverdrup circulation, and find a very broad and zonal flow and underflow off their west Australian coast. The latter apply wind stress curl to yield a realistic Sverdrup flow; their solution features a more concentrated flow/underflow pair curving northwest then west from Cape Leeuwin, rather similar to that in the present model.

The above mechanism may be operating in all of the present runs, including that with the passage closed, since the Sverdrup circulation off the western Australian coast is unchanged. Indeed, the total velocity fields of all runs show a flow/underflow pair with similar trajectory (HG). This feature is simply strengthened, more or less in situ, in the presence of an Indonesian Throughflow.

First mode motions are relatively unaffected by the Sverdrup flow because the first mode is faster and deeper, and because the Sverdrup flow itself has vertical structure roughly like that of the first mode (plus a weak barotropic component). The meridional boundaries of the first mode–like response (Fig. 14a) roughly coincide with the barotropic flow response (Fig. 6c or HG's Fig. 11a), which acts to cancel the deep return baroclinic currents.

Examination of Fig. 9 reveals two further exceptions to the simple modal view. First, the flow/underflow pair extends westward much more rapidly than would be expected for a freely propagating second mode Rossby wave. The rapid extension appears linked to westward advection of upper-ocean density perturbations at latitudes 15° to 20°S, primarily by motion associated with the first mode signal and with the background South Indian Equatorial Current. Westward motions in the upper ocean associated with both features are of order 0.05 m s^{-1}, which is similar to the propagation speed of the second mode. Substantial enhancement is therefore expected for the extension rate of second mode–like features across the Indian Ocean.

Figures 9a,b also reveal that the leading edge of the Indian Ocean temperature signal is associated with a strong surface flow but little reverse underflow. This is inconsistent with the first mode velocity profile. However, the underflow in the full model would be subject to viscous and pressure drag associated with the bottom topography, and also a weak linear bottom friction. To check the effect of deep-ocean flow retardation, the "first internal mode" experiment was rerun with the simplified model, but with a very large coefficient of bottom friction (C_B = 2, cf. Table 2 of HG). The response at 9 months is quite similar to that in Fig. 9a, with the reverse underflow largely absent. A reverse deep underflow develops later, but remains weak. However, the final upper-ocean temperature and current responses for both "first internal mode" experiments are very similar.

Another exception to the simple modal view is revealed by examination of thermal adjustment timescales in the Indian Ocean. Figure 15 shows the temperature averaged over the south Indian Ocean (10°–40°S, 20°–115°E) at 215 and 1025 m as functions of time following the opening of the Indonesian passage in the full model. Also shown are the corresponding averaged temperatures from the simplified model in the case of first mode forcing. We see that upper-ocean temperatures adjust on a timescale roughly similar to that expected for the first mode. In contrast, a substantial part of the deeper level adjustment occurs on much longer timescales, so that adjustment is far from complete even after 20 years. The thermodynamics of the deep-ocean adjustment in the full model were investigated by separating horizontal and vertical advection effects at 1025 m, as per Fig. 7. Both horizontal and vertical advection changes contribute positively to the development and maintenance of the deep temperature perturbation in the open ocean, during the entire course of adjustment. However, the (initially dominant) vertical advection changes diminish steadily with time, so that after about 10 years horizontal advection changes become dominant. (Both advection changes remain large and have mixed sign near the continental boundaries.) Thus, neither in timescale nor

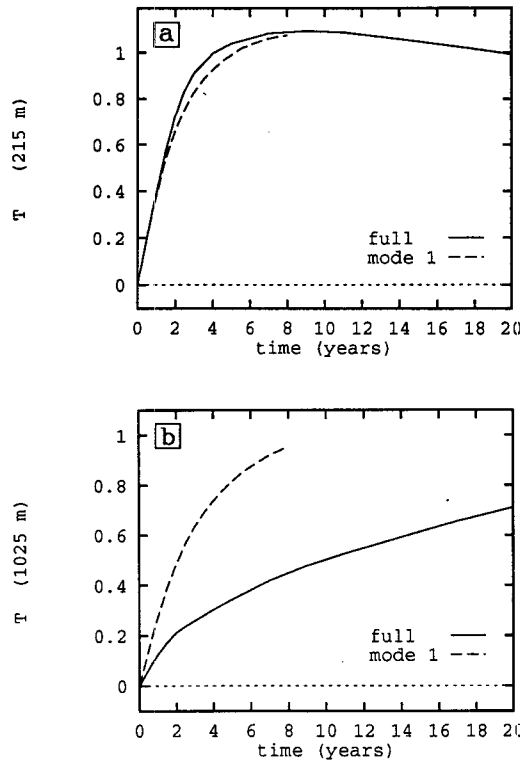

FIG. 15. Temperature perturbation at (a) 215-m and (b) 1025-m depth averaged over the south Indian Ocean (10°–40°S, 20°–115°E) as function of time following opening of the Indonesian passage in the full model (solid) and switch on of first mode forcing in the simplified model (dashed). Values have been divided by the respective final equilibrium temperature change prior to plotting.

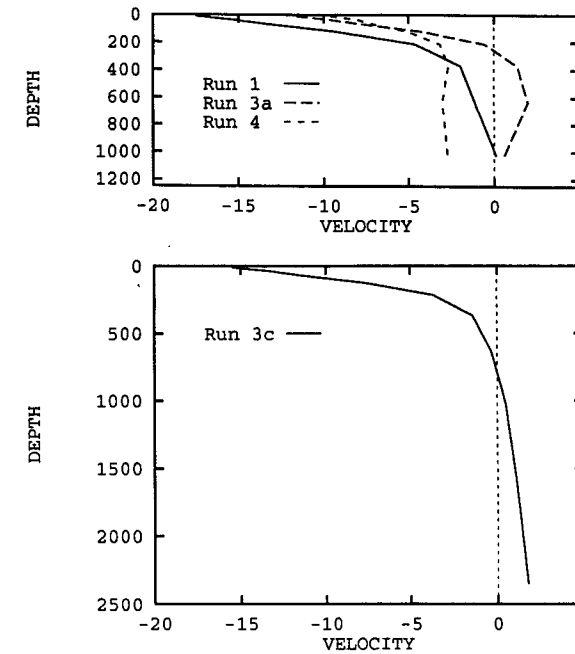

FIG. 16. Vertical profiles of flow across 120°E between Indonesia and Australia, in four equilibrium cases of HG. Values were obtained by summing the velocities at grid points across the passage, for each level. Negative values indicate westward flow.

thermodynamics is the latter part of the deep adjustment consistent with simple modal adjustment.

Finally, we note that the simple modal view is somewhat idealized in that it does not, for example, take account of the effect of meridional variation in density profile. A more detailed picture of the adjustment dynamics might be obtained by appropriate experiments with a buoyancy/mass-forced thermocline model like that of Luyten and Stommel (1986) or McCreary et al. (1992). Such work is beyond the present scope of this paper.

Despite the above exceptions and limitations, modal theory provides a useful framework for interpreting the model response to changes in the throughflow. In particular, it is possible to interpret the differences between the several throughflow runs of HG in terms of the vertical mode response. Figure 16 shows the profiles of throughflow transport for four of HG's runs. Table 3 gives the projections of these profiles onto the first and second mode profiles of Figs. 10a and 10c. Hirst and Godfrey's runs 1, 3c, and 4 all have throughflow projecting strongly onto the first mode, and all displayed basinwide deep warming, and enhancement of the Agulhas Current and associated heat loss. In contrast, the throughflow in run 3a projects only weakly onto the first mode, and the above basinwide effects are also weak. Meanwhile, runs 1, 3a, and 3c all have throughflow projecting strongly onto the second mode, and all display marked strengthening of the flow/underflow pair and associated heat loss near the western Australian coast. Run 4, which features near-zero projection of the throughflow onto the second mode, does not display any significant change in the flow/underflow pair and associated heat loss from that in the passage-closed case. This modal interpretation of the disparate responses in HG follows closely from the discussion of McCreary and Kundu (1986) of their simple model results.

The potential effect of model and forcing imperfections on the response were discussed in HG. We simply comment here on the possible effect of using a smaller vertical diffusivity, which would yield a shallower, more realistic, vertical density structure. In such a case, the

TABLE 3. Coefficients (c_1, c_2) for the projection of each of the throughflow profiles in Fig. 16 onto the internal mode profiles of Figs. 10a and 10c.

Run (of HG)	c_1	c_2
1	−5.2	−3.8
3a	−1.1	−2.7
3c	−4.4	−4.3
4	−4.3	−0.4

associated modal structure would also shoal and the modal wave speed may also decrease modestly. The Sverdrup circulation may also shoal; however, it would remain constant in terms of volume transport (provided the wind stress forcing was unchanged), in which case upper-ocean velocities must increase (e.g., Hirst and Cai 1994). Therefore, we may expect the shallower slower modes to be more strongly affected by the shallower swifter Sverdrup circulation. Consequently, second and higher mode penetration may be more strongly blocked.

6. Summary

This paper investigates the timescales and mechanisms of subsurface temperature response in a global GCM for the case of a sudden change in Indonesian Throughflow. It therefore attempts to provide a more complete picture of mechanisms of remote *surface* response, since it was shown in HG that the surface response is crucially dependent on the pattern of the subsurface temperature response. Two experiments are conducted with the full model. The first is a large-perturbation experiment where the passage is suddenly opened. The second is a small-perturbation experiment where the throughflow of the equilibrated passage-open solution is slightly enhanced by an applied body force such that the relative vertical profile of the flow is preserved.

In both runs, the transient subsurface response is mostly dominated by features reminiscent of propagating internal wave fronts. These features are primarily responsible for setting up the basinwide subsurface temperature changes in the Pacific and Indian Oceans noted by HG in the final equilibrium. Development of large SST responses in several of the regions reported by HG occurred only after arrival of such subsurface features.

The pattern and thermodynamics of the response suggest important contributions to the basinwide response from components akin to the first and second internal modes. To further investigate the relevance of internal mode adjustment, a comparison is made between the full model solution and solutions of a simplified model featuring a flat bottom and a background state that is horizontally uniform and at rest. The simplified model is subject to idealized forcings in the Indonesian passage, designed to excite in turn the first and second internal modes. The response to the first mode forcing is quantitatively similar to that apparent for the first mode–like component of the full model response, the major exception being in the vicinity of the Antarctic Curcumpolar Current, where the full model response does not penetrate as far south. The response to the second mode forcing differs more significantly from the second mode–like component of the full model response. The discrepancies are attributed partly to horizontal advective effects in the full model. In particular, it appears that the background Sverdrup circulation prevents penetration of the (slow) second mode signal into large parts of the subtropical and midlatitude ocean interiors. In addition, the second mode–like signal suffers strong erosion in regions of convective mixing and surface heat loss such as near Cape Leeuwin.

Two major exceptions to the internal modal picture are noted. First, the large response in the Tasman Sea develops steadily as a result of horizontal advection changes in the upper 800 m. Second, the deep temperature response in the Indian Ocean appears partly as the result of slow advective processes, resulting in an adjustment timescale much longer than that expected from internal mode adjustment alone. The effect of this slow deep adjustment on the surface SST and heat flux fields appears small, except possibly in the eastern part of the Agulhas Outflow region (cf. Figs. 8 and 16).

The large and small perturbation experiments with the full model yield very similar changes, after scaling. This shows that the model response is nearly linear with respect to a change in magnitude of throughflow. The overall pattern of response is broadly fixed provided that the relative profile of the throughflow transport is unchanged. In contrast, major changes occur in the pattern of response if the throughflow profile changes. These changes are interpreted as resulting from excitation of a different mix of vertical modes.

The pattern of response may also be significantly affected by the frequency of a periodic change in the throughflow, such as that associated with the annual or El Niño/Southern Oscillation (ENSO) cycles. A high-frequency variation in the throughflow would tend to have large surface effects only in those regions where the effects develop quickly following a change (e.g., equatorial Pacific, Tasman Sea, and Leeuwin Current regions). Those regions showing very slow or delayed response to a throughflow change (e.g., much of the Agulhas Outflow) would be expected to be little affected by throughflow variation of period less than a few years.

In conclusion, we summarize that the full model's response to a change in the Indonesian Throughflow features extensive subsurface temperature changes across both the Pacific and Indian Oceans, which are induced primarily by baroclinic adjustment approximating the propagation of internal mode signals, especially of the first and second modes. Over most of the oceans, such signals are largely insulated from the surface relaxation conditions on temperature and salinity (because of the small vertical diffusivity) and so may travel great distances from their source. Only when the signals encounter deep convective mixed layers or strong upwelling is their heat brought to the surface and lost to the atmosphere. The present results, and those of HG, illustrate a mechanism of remote oceanic response that may have a wider application than to just the special case of changed throughflow. Namely,

regions of convective mixing or strong upwelling are identified as "sensitive regions" that are liable to show a relatively large *surface* response to any remote change in surface forcing or ocean model geometry capable of generating subsurface baroclinic adjustments that are able to propagate to the particular sensitive region. For example, we have run a very simple wind forcing experiment where the full model in equilibrium in the passage-open case was subject to a perturbation wind stress in the equatorial Pacific for 12 months. The strongest SST responses outside the tropical Pacific were in the relatively remote far southeast and far north Pacific, in regions identified in HG as having deep convective mixed layers (though the responses there attained a magnitude only one-quarter the size of the SST perturbations off the Peru/Equador coast). The idea of remote response via internal wave forcing is, of course, familiar to the ENSO community in the context of remotely forced warming in the upwelling zones of the eastern tropical Pacific.

Acknowledgments. The authors would like to thank Drs. R. L. Hughes and A. M. Moore for constructive reviews of a preliminary draft. Thanks also to Drs. W. J. Cai and H. Granek for assistance with graphics. The computations were carried out on the CRAY-YMP-2 at the Joint Supercomputer Facility, Port Melbourne, Victoria. This research was partly funded by the Wool Research and Development Corporation of Australia.

REFERENCES

Anderson, D., and A. E. Gill, 1975: Spin-up of a stratified ocean with application to upwelling. *Deep-Sea Res.*, **22**, 583–596.

Bryan, K., 1984: Accelerating the convergence to equilibrium of ocean–climate models. *J. Phys. Oceanogr.*, **14**, 666–673.

Cox, M. D., 1984: A primitive equation, 3-dimensional model of the ocean. GFDL Ocean Group Tech. Rep. No. 1, GFDL/Princeton University, Princeton, NJ, 141 pp.

Esbensen, S. K., and V. Kushnir, 1981: The heat budget of the global ocean: An atlas based on estimates from surface marine observations. Climatic Research Institute Report 29, Oregon State University, Corvallis, OR, 27 pp.

Gill, A. E., 1982: *Atmosphere–Ocean Dynamics.* Int. Geophys. Ser., Vol. 30, Academic Press, 662 pp.

Godfrey, J. S., 1989: A Sverdrup model of the depth-integrated flow for the World Ocean allowing for island circulations. *Geophys. Astrophys. Fluid Dyn.*, **45**, 89–112.

——, and T. J. Golding, 1981: The Sverdrup relation in the Indian Ocean and the effect of the Pacific–Indian Ocean throughflow on Indian Ocean circulation and on the east Australian Current. *J. Phys. Oceanogr.*, **11**, 771–779.

——, and A. J. Weaver, 1991: Is the Leeuwin Current driven by Pacific heating and winds? *Progress in Oceanography,* Vol. 27, Pergamon, 225–272.

——, A. C. Hirst, and J. L. Wilkin, 1993: Why does the Indonesian Throughflow appear to originate from the North Pacific? *J. Phys. Oceanogr.*, **23**, 1087–1098.

Hellerman, S., and M. Rosenstein, 1983: Normal monthly wind stress over the World Ocean with error estimates. *J. Phys. Oceanogr.*, **13**, 1093–1104.

Hirst, A. C., and J. S. Godfrey, 1993: The role of Indonesian Throughflow in a global ocean GCM. *J. Phys. Oceanogr.*, **23**, 1057–1086.

——, and W.-J. Cai, 1994: Sensitivity of a World Ocean GCM to changes in subsurface mixing parameterization. *J. Phys. Oceanogr.*, **24**, 1256–1279.

Hughes, T., A. J. Weaver, and J. S. Godfrey, 1992: Thermohaline forcing of the Indian Ocean by the Pacific Ocean. *Deep-Sea Res.*, **39**, 965–996.

Levitus, S., 1982: *Climatological Atlas of the World Ocean.* NOAA Prof. Paper 13, U.S. Govt. Printing Office, Washington, D.C., 173 pp.

Luyten, J. R., and H. Stommel, 1986: Gyres driven by combined wind and buoyancy flux. *J. Phys. Oceanogr.*, **16**, 1551–1560.

——, J. Pedlosky, and H. Stommel, 1983: The ventilated thermocline. *J. Phys. Oceanogr.*, **13**, 292–309.

McCreary, J. P., 1980: Modelling wind-driven circulation. Hawaii Institute of Geophysics Rep. HIG-80-3, 64 pp.

——, and P. K. Kundu, 1986: On the dynamics of the throughflow from the Pacific to the Indian Ocean. *J. Phys. Oceanogr.*, **16**, 2191–2198.

——, Y. Fukamachi, and P. Lu, 1992: A nonlinear mechanism for maintaining coastally trapped eastern boundary currents. *J. Geophys. Res. (Oceans)*, **97**, 5677–5692.

Moore, D. W., and S. G. H. Philander, 1977: Modeling of the tropical ocean circulation. *The Sea,* Vol. 6, E. D. Goldberg, I. N. McCave, J. J. O'Brien, and J. H. Steele, Eds., Wiley-Interscience, 319–362.

Munk, W. H., 1950: On the wind-driven ocean circulation. *J. Meteor.*, **7**, 79–93.

Rhines, P. B., and W. R. Young, 1982: A theory of the wind driven circulation. I. Mid-ocean gyres. *J. Mar. Res.*, **40**(Suppl.), 559–596.

Wajsowicz, R. C., 1986: Free planetary waves in finite-difference numerical models. *J. Phys. Oceanogr.*, **16**, 773–789.

——, and A. E. Gill, 1986: Adjustment of the ocean under buoyancy forces. Part I: The role of Kelvin waves. *J. Phys. Oceanogr.*, **16**, 2097–2114.